Journal of Hydrology: Regional Studies 64 (2026) 103310

Contents lists available at ScienceDirect

Journal of Hydrology: Regional Studies

journal homepage: www.elsevier.com/locate/ejrh

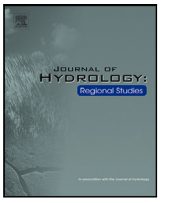

Long-term projections of coastal drainage under climate change and relative sea-level rise for coastal basins of Ravenna, northeastern Italy

Matteo Meli *, Marco Antonellini, Beatrice Maria Sole Giambastiani

Department of Biological, Geological and Environmental Sciences, University of Bologna, Via Zamboni 67, Bologna, 40126, Italy

ARTICLE INFO

Dataset link: https://simc.arpae.it/dext3r/, https://doi.org/10.5281/zenodo.14671018, https://servizi-gis.arpae.it/Html5Viewer/index.html?locale=it-IT&viewer&viewer=Geoportal.Geoportal, https://climateknowledgeportal.worldbank.org/country/italy/climate-data-projections, https://sealevel.nasa.gov/data_tools/17

Keywords:
Coastal basin
Drainage
Sea-level rise
Land subsidence
Time series analysis
Climate change
Ravenna

ABSTRACT

Study region: The Ravenna coastal plain (northeastern Italy, Po River plain).

Study focus: This study analyzes the long-term evolution of land-reclamation pumping, focusing on the Quinto and Rasponi low-lying polder basins (1977–2023), and quantifies the relative influence of hydroclimatic variability versus relative sea-level change. A non-parametric signal decomposition and multivariate dynamic regression are used to separate oscillatory variability from residual trends and to propagate the trend component under scenario-based projections through 2100.

New hydrological insights for the region: Hydroclimatic variability contributes primarily to interannual-to-decadal fluctuations in pumping, while exerting little influence on the long-term trend. In contrast, relative sea-level rise explains most of the persistent increase in pumping demand. Projections indicate that the contribution of vertical land motion to relative sea-level change is expected to decrease as subsidence rates have been decelerating and will stabilize at constant values, whereas geocentric sea-level rise becomes increasingly dominant, implying growing drainage requirements toward 2100 and increasing challenges for maintaining dry conditions and protecting freshwater resources in the Ravenna coastal basins.

1. Introduction

Low-lying coastal regions, such as the Po delta area in northeastern Italy, are particularly vulnerable to the combined pressures of climate change (Syvitski et al., 2022; IPCC, 2023), land subsidence (Tosi et al., 2010; Teatini et al., 2011; Fiaschi et al., 2017), sea-level rise (Da Lio and Tosi, 2019; Meli et al., 2021), and decreased freshwater availability (Maicu et al., 2018; Giambastiani et al., 2021; Luo et al., 2024). These driving forces interact by altering hydrological systems, especially changing the patterns and magnitude of artificial drainage in coastal polder basins, thereby increasing vulnerability to flooding (Alifu et al., 2022; Cremonini et al., 2024; Valente et al., 2025) and storm surges (Wong et al., 2014; Ciavola et al., 2007) with severe ecological and socioeconomic implications (Alexandrakis et al., 2015).

The coastal plain of Ravenna, located along the northern Adriatic Sea, suffers such vulnerability. Originally designed to enable land reclamation and agricultural productivity, the drainage infrastructure of the area, made of a complex network of pumping stations and drainage canals, plays an important role in flood prevention and water table control. However, its operation is challenged by long-term hydroclimatic shifts, topography below mean sea level, and subsidence, which together compromise the sustainability of water management in the coastal area. Current projections (Perini et al., 2017) suggest that under high-end

* Corresponding author.
E-mail address: matteo.meli7@unibo.it (M. Meli).

https://doi.org/10.1016/j.ejrh.2026.103310
Received 1 September 2025; Received in revised form 27 February 2026; Accepted 28 February 2026

scenarios, combined with local sea-level change (Meli et al., 2021) and ongoing subsidence (Antonellini et al., 2019), and in the absence of adaptation measures, large portions of the Ravenna territory may progressively fall below mean sea level by 2100.

Previous studies on this coastal plain (Giambastiani et al., 2020; Soboyejo et al., 2021) have highlighted how mechanical drainage, along with land subsidence and seepage processes, has significantly contributed to the salinization of the shallow coastal aquifer. In particular, drainage trends have shown persistent increases over the last five decades, with evidence of geophysical drivers (i.e., subsidence-induced vertical gradients) as the main causes, while climatic influences, such as rising temperatures, increased drought frequency, and altered precipitation regimes, appear to have had a secondary effect on long-term drainage dynamics.

Despite these advances, a systematic assessment of the coupled effects of long-term climatic forcing and local sea-level trends on drainage evolution is still lacking. The long-term efficiency of the drainage system is likely to decline, particularly considering projected sea-level rise. While subsidence in the Ravenna area is no longer as severe as in the past (Teatini et al., 2005, 2006; Antonellini et al., 2019), the relative lowering of the land, which results from the combination of residual subsidence and the rising sea level, is a relevant issue. This means that even with stable ground levels, sea-level rise will reduce the efficiency of the drainage system, leading to higher energy demands, more frequent interventions, and increased vulnerability (Titus et al., 1987; Habel et al., 2020; Obara et al., 2025).

In this context, the present work expands the historical analysis of drainage time series by integrating nearly five decades of drainage, hydroclimatic, and sea-level data with advanced signal decomposition techniques and multivariate dynamic regression modeling. The study aims to assess the relative contributions of climate variability (precipitation, evapotranspiration) and geophysical processes (land subsidence and sea-level change) on the evolution of pumping rates and to develop local projections of pumping requirements throughout the 21st century. Understanding the temporal interactions among these processes is critical for sustainable water management. Under future climate scenarios, projected increases in temperature, altered precipitation patterns, and accelerated sea-level rise are expected to further intensify drainage demand. These changes will require targeted strategies to adapt existing drainage infrastructure to changes in land elevation, rising sea level, and shifting hydraulic gradients to maintain effective flood protection in low-lying coastal zones.

2. Study area

The study area includes two coastal basins, Quinto and Rasponi, in the southern low-lying coastal plain of the Municipality of Ravenna (Fig. 1). These coastal basins are part of a larger network of 15 drainage basins and are morphologically similar to Dutch polders, characterized by artificially drained lowlands enclosed by embankments, mostly located below mean sea level, and dependent on mechanical pumping systems to regulate groundwater and surface water levels in support of agricultural productivity and urban development. Higher elevations (about 3–5 m a.s.l.) are recorded only along palaeodunes and current coastal dunes. Drainage operations are managed by the Land Reclamation Consortium, which maintains a complex system of canals, ditches, sluices, and pumping stations designed to keep the water table at a threshold of 1.5–2.0 m below ground level throughout the year. The pumping stations are automatically activated when the water level in the drainage channels reaches the threshold, regardless of soil water availability or weather forecasts. The pumping stations are typically located inland, several kilometers from the shoreline (Fig. 1), and the drainage, therefore, creates a hydraulic gradient directed inland (Antonellini et al., 2008). The channel network supports drainage during autumn and winter, and irrigation during spring and summer.

The Quinto basin is the largest low-lying basin in the area (approximately 9200 ha, 10% of the Ravenna province), located between the Fiumi Uniti River in the north and the Bevano River in the south (Fig. 1). The basin includes coastal urban areas, coastal and historical pine forests, agricultural land, and several active and abandoned gravel quarries that form lakes (Greggio et al., 2012; Mollema et al., 2011). The main pumping station is located about 5 km from the coastline, while two other secondary stations (Fig. 1) are present and operate for safety reasons in the event of significant precipitation, conveying water to the main one. The Rasponi basin is smaller (2600 ha) and mostly supports agricultural activities. The limited size results in a shorter hydrological response time than the Quinto basin. Rasponi serves the entire coastal area of Lido di Adriano, which lies at a low elevation and has suffered a higher rate of subsidence than the Quinto Basin.

Geologically, the area consists of a Quaternary sedimentary sequence composed of beach and dune sands interbedded with lagoonal silt, clay, and peat layers, representing a dynamic barrier-lagoon-estuarine depositional system (Campo et al., 2017). The shallow coastal aquifer comprises two sandy units separated by low-permeability prodelta deposits. The upper sandy unit, which is hydraulically connected to the drainage network, ranges in thickness from 5 to 10 m (Giambastiani et al., 2020). The region has experienced substantial land subsidence over the past century, initially driven by extensive groundwater and hydrocarbon extraction (Teatini et al., 2005, 2006). Recent analyses have also highlighted spatially heterogeneous subsidence hotspots in the Ravenna coastal plain, with higher rates in reclaimed areas and locally associated with the building-induced loading effects (Verberne et al., 2025). This pattern reflects a combination of shallow compaction influenced by drainage and a localized onshore contribution from the offshore gas-extraction-related subsidence bowl, with smaller secondary roles for drainage practices and groundwater withdrawal (Verberne et al., 2025). Although mitigation measures introduced in the 1980s have reduced extraction-induced subsidence, residual subsidence rates of 5–10 mm/yr persist, particularly in coastal sectors (Bitelli et al., 2015; Antonellini et al., 2019; Soboyejo et al., 2021). This process has changed the hydraulic gradient between the aquifer and the drainage canals, enhancing saltwater up-coning and altering groundwater flow patterns (Giambastiani et al., 2020).

The area is characterized by a temperate climate (average yearly temperature of ca. 14 °C) with moderate precipitation (about 600 mm/yr) and interannual variability (Mollema et al., 2011). Long-term meteorological records show increasing temperature trends and the occurrence of prolonged droughts (Meli and Romagnoli, 2022), which reduce recharge and amplify seasonal imbalances in the water budget. These dynamics, combined with subsidence and sea-level rise, enhance the complexity of managing surface and groundwater systems in this sensitive coastal zone.

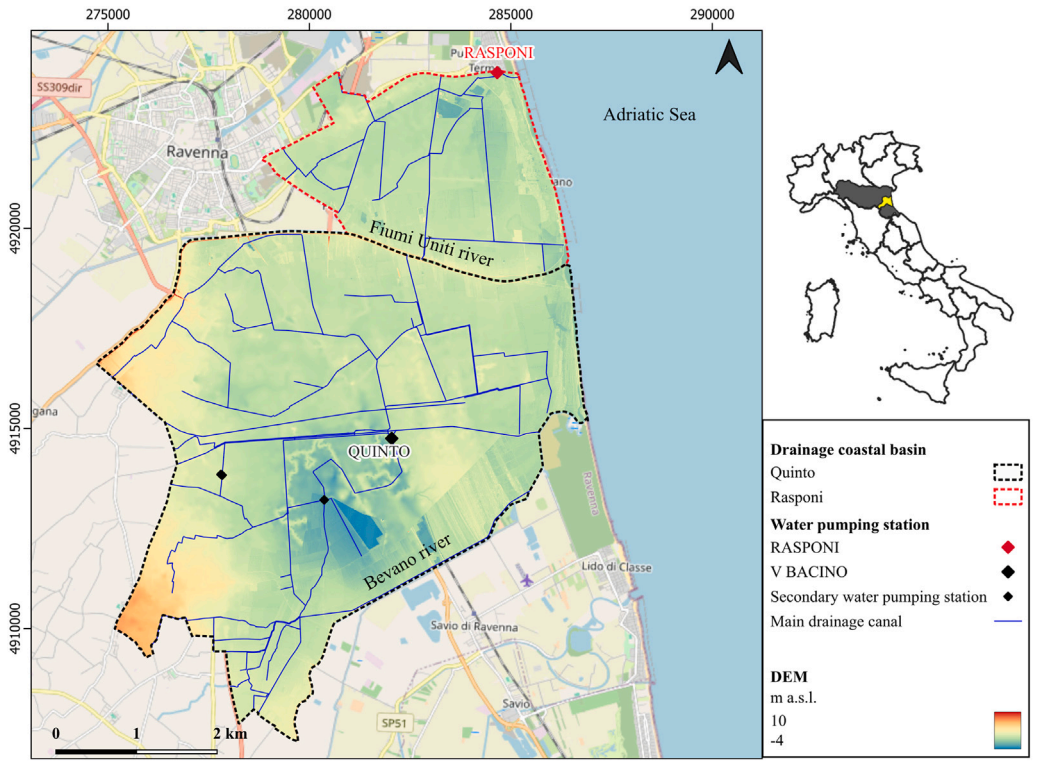

Fig. 1. The low-lying coastal area of Ravenna (yellow area in the upper right panel) and the Quinto (black dashed line) and Rasponi (red dashed line in the left panel) within the Emilia-Romagna Region (gray area in the upper right panel), northeastern Italy. Map coordinate system: WGS84-UTM Zone 33N. Cartographic basemap from Google Maps. Elevation data are based on a 5 × 5 m resolution DEM, generated from a 2009 LiDAR acquisition by the Emilia-Romagna Region (available at https://geoportale.regione.emilia-romagna.it/download/download-data?type=raster).

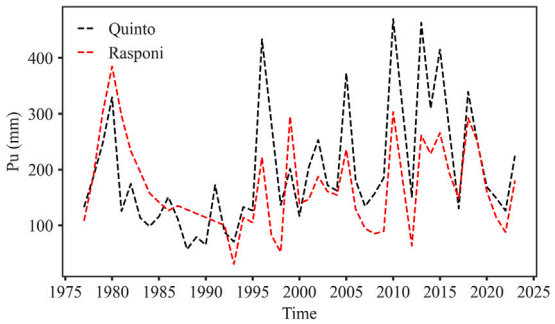

Fig. 2. Annual time series of pumping records in the Quinto (black dashed line) and Rasponi (red dashed line) basins from 1977 to 2023.

3. Materials and methods

3.1. Data

Annual pumping (P_u) records for the Quinto and Rasponi coastal basins (Fig. 2) were manually digitized from the original bookkeeping data. The available series span 1971–2023 and were processed following Soboyejo et al. (2021), yielding equivalent water-column depths (mm) by dividing the total drained volume (m^3) by basin area (m^2). To ensure consistency with the other datasets, all records prior to 1977 were excluded. Finally, given that the Rasponi record has a four-year gap (1988–1991), missing values were filled by linear interpolation.

Daily local precipitation (P) and air temperature (T) data from 1977 to 2023 were retrieved from the meteorological station located in the Ravenna municipality via the Arpae DEXT3R database (https://simc.arpae.it/dext3r/) and subsequently aggregated to annual values (Fig. 3a and Fig. 3b). Missing data were filled using records from the nearest weather stations. Based on these data,

the annual actual evapotranspiration (Etr; Fig. 3c) was computed using the Turc method (Turc, 1951; Gudulas et al., 2013):

$$Etr = \frac{P}{\sqrt{\frac{P^2}{(300+25T+0.05T^3)^2} + 0.9}} \quad (1)$$

where Etr is the annual actual evapotranspiration (mm), P is the annual precipitation (mm), and T is the mean annual air temperature (° C). The hydrologic budget of a polder basin (Vlotman et al., 2020), like Quinto and Rasponi, is given by:

$$P + Q_v = P_u + Etr \pm \Delta S \quad (2)$$

where Q_v represents vertical and horizontal seepage (mm) and P_u represents land reclamation pumping (mm). The change in storage, ΔS (mm), over the multi-annual period considered in this study can be assumed to be negligible, as the unsaturated-zone thickness is artificially controlled and kept approximately constant to support agricultural activities, limiting long-term changes in soil storage.

The local geocentric sea-level (GSL) time series, representing sea-level variations relative to the Earth's center of mass (Gregory et al., 2019), was obtained from Meli et al. (2025) for the period 1993–2020. To extend the record back to 1977 and up to 2023 (Fig. 3e), the dataset was processed following the methodology outlined in Meli et al. (2026). This dataset describes how local GSL evolved over the period under analysis due to changes in water density, circulation, and mass redistribution. However, a critical factor influencing local sea-level variability is vertical land movement (VLM), especially in low-lying areas, such as the Emilia-Romagna coastal region, where subsidence processes can locally amplify the magnitude of GSL by 50% to over 600% (Meli et al., 2025). Thus, it is crucial to consider the combined interaction of the two processes, commonly referred to as relative sea-level change (RSL), which in its simplest form (Farrell and Clark, 1976) is expressed as $RSL = GSL - VLM$.

Annual VLM rates for the Rasponi and Quinto basins were obtained for the period spanning 1977 to 2023 from available information, in terms of eight predefined intervals, each representing a distinct temporal phase of VLM behavior. In detail, periods 1977–1982, 1982–1986, and 1986–1992 are from Teatini et al. (2005); 1992–2000 and 2002–2006 are from the Arpae Geoportal (https://servizi-gis.arpae.it/Html5Viewer/index.html?locale=it-IT&viewer&viewer=Geoportal.Geoportal); while 2006–2012, 2012–2016, and 2016–2021 are from Meli et al. (2025). In each basin, VLM was calculated for each interval either by averaging the available values within the domain (for data after 1992) or by considering isokinetic lines and the corresponding enclosed areas (for data prior to 1992). Thus, local annual cumulative VLM time series (Fig. 3f) were reconstructed by sequentially aggregating these interval rates, with annual velocities computed as year-over-year differences relative to a fixed datum set to zero in 1977. To avoid gaps, trends for the years 2000–2001 and 2022–2023 were assumed to be consistent with those of the periods 2002–2006 and 2016–2021, respectively.

The P_u term in polder basins is partly controlled by short-term climate conditions such as intense P events or extended drought periods, which impart a strong seasonal and interannual variability, and by a background trend including the $P - Etr$ trend (Fig. 3d) and the horizontal and vertical seepage trend, which is controlled by the difference in elevation between GSL and the top of the water table in the polder basin (de Louw et al., 2011; Vlotman et al., 2020). Any change in RSL translates into a change in hydraulic head (H) that influences the seepage term (Q_v) and consequently the background (non-climate-related) P_u trend. As a result, the change in Q_v is related to H in a first approximation by Darcy's law (Vlotman et al., 2020):

$$\Delta Q_v = K\frac{\Delta H}{L} \quad (3)$$

where K (m/d) is an average of the horizontal and vertical hydraulic conductivity (vertical component prevalent) and L is the saturated thickness of the unconfined/semi-confined shallow aquifer. Giambastiani et al. (2020) estimated a representative value of K for the area to be 0.03 m/d and L to be approximately 23 m. Using these values, the change in basin inflow can be estimated (converted to annual depth units, mm/yr) as reported in Tables A1 and A2 and compared with the measurements. The analysis of discrepancies (i.e., $\Delta P_u - \Delta Q_v$) provides insight into the differing hydraulic behaviors of the basins. The contribution of Q_v should not be included as a separate time series in the analysis, as it is already implicitly accounted for through the effect of RSL, which directly influences Q_v dynamics. Including Q_v as an independent variable would result in double counting its influence on P_u behavior. In contrast, all other variables, such as P and T, should be included in the multivariate analysis, as they are independent from VLM and GSL change.

3.2. Local projections

Annual climate projections of local P (Fig. 3a) and mean surface T (Fig. 3b) were retrieved from the Italian section of the Climate Change Knowledge Portal (https://climateknowledgeportal.worldbank.org/country/italy/climate-data-projections). The data cover the period 2014–2100 and are provided as a multi-model ensemble based on the global climate models from the Sixth Phase of the Coupled Model Intercomparison Project (CMIP6), which also forms the scientific basis of the IPCC's Sixth Assessment Report (IPCC, 2023). These projections represent the most probable future evolution of the climate system under specific Shared Socioeconomic Pathways (SSPs). SSPs are defined by different trajectories of emissions, technological development, governance, mitigation efforts, demographics, and economic growth, which together drive possible future climate scenarios. In detail, four scenarios were considered in this work: SSP1-2.6, SSP2-4.5, SSP3-7.0, and SSP5-8.5. The number following the dash indicates the approximate level of radiative forcing (in $W \cdot m^{-2}$) projected by the end of the 21st century relative to the preindustrial period. SSP1-2.6 is commonly regarded as the most optimistic pathway, assuming strong mitigation efforts and the achievement of net-zero emissions in the second half of the century. In contrast, SSP5-8.5 represents the most pessimistic scenario, assuming high greenhouse

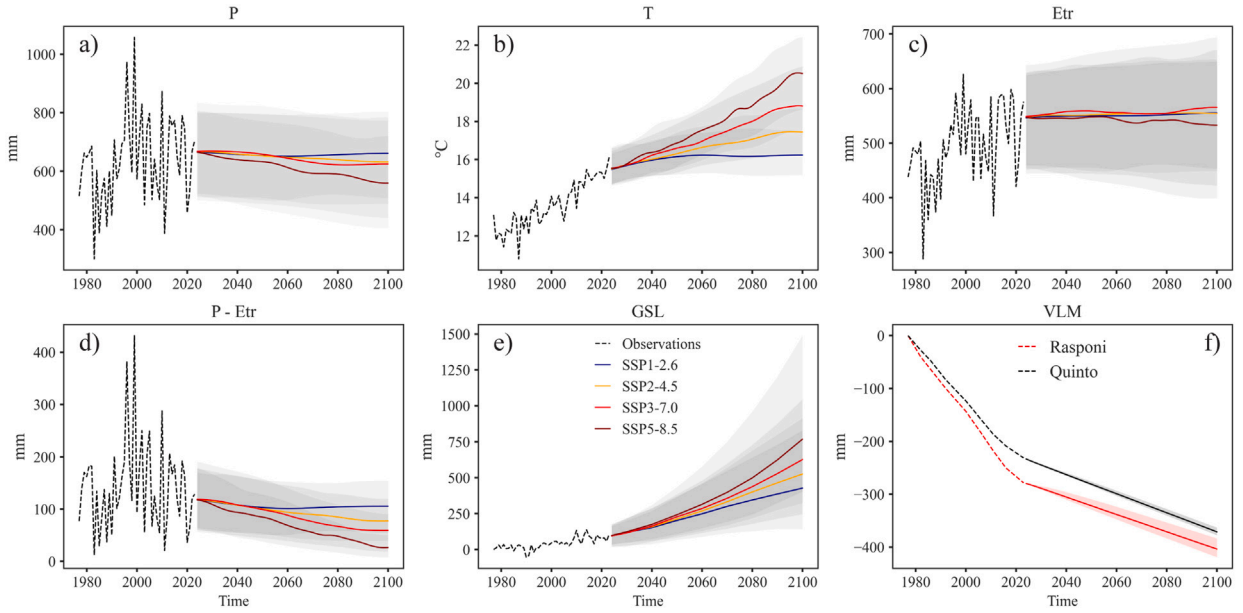

Fig. 3. Dashed lines represent annual time series from local observations (1977–2023) of P (a), T (b), Etr (c), $P-Etr$ (d), GSL (e), and VLM (f). Projections for the period 2024–2100 (details in Section 3.2) are provided according to the Shared Socioeconomic Pathways (SSPs), as outlined in the Intergovernmental Panel on Climate Change's Sixth Assessment Report (IPCC, 2023). Color codes, shown in panel (e), apply to all panels (a–e) and refer to the median (50th percentile) of the projections, while gray shaded areas represent the upper (90th percentile) and lower (10th percentile) bounds of each distribution. Projections of VLM (panel f) are presented as the 50th percentile (solid lines), with the 10th and 90th bounds shown as shaded areas, for the Quinto (black) and Rasponi (red) basins.

gas emissions in the absence of climate policy interventions (see O'Neill et al., 2017 for details). It should be noted that another scenario, SSP1-1.9 (representing a pathway with net-zero emissions achieved around the middle of the 21st century), has also been formulated within the SSP framework but is not considered in this study.

Future GSL scenarios (Fig. 3e), representing the projected sea-level rise for the period 2020–2100 under the four SSPs considered in this study, were obtained from Fox-Kemper et al. (2021) and extracted using the NASA Sea Level Projection Tool (https://sealevel.nasa.gov/data_tools/17), selecting the closest pixel (44° N; 13° E) of the multi-model ensemble to the study area in the northern Adriatic Sea. These projections, along with their associated confidence ranges, incorporate uncertainties related to both future T changes, driven by emission scenarios, and the complex relationship between T and the various contributors to GSL rise, such as ice loss from glaciers and ice sheets, ocean dynamics, and thermal expansion.

To ensure consistency with local observational data, all climate projections were corrected using standard bias adjustment techniques. These adjustments were necessary to align future scenarios with present-day local conditions, enabling a more realistic assessment of system responses. The P and T projections were originally available as spatial averages over the entire Emilia-Romagna region, which includes coastal areas, plains, and inland mountainous zones. As a result, discrepancies arose due to the spatial mismatch between the regional-scale projections and the smaller coastal basins under investigation. A similar issue applies to GSL, where modeled trajectories may not capture the pronounced interannual variability observed locally in recent decades. To address this, an additive correction was applied to T data, based on the mean difference between observed and projected values over the 2014–2023 period. For P, a multiplicative scaling factor was used, derived from the ratio of observed to projected means over the same reference period. The GSL projections, originally expressed as anomalies relative to the 1995–2014 baseline, were adjusted by anchoring the median scenario to the mean observed during the overlapping years (2020–2024). These corrections ensure a consistent transition between historical observations and future projections, which is critical for local-scale impact assessments. Aligning all variables to a recent observational baseline enhances the applicability of climate scenarios as forcing inputs in empirical or process-based models.

To estimate long-term VLM trajectories through 2100, the observed annual rates were decomposed into a deterministic component and a stochastic residual. The deterministic trend was modeled using a second-order polynomial regression to capture the observed and literature-supported deceleration in VLM over recent decades (Marcaccio and Mazzei, 2023). Although statistical indicators such as the Akaike Information Criterion (AIC; Akaike, 1974) and the Bayesian Information Criterion (BIC; Schwarz, 1978) suggested that a linear model might provide a slightly more parsimonious fit for the Rasponi basin, the quadratic form was retained for both basins. This approach better represents the expected nonlinear slowdown of VLM following the enforcement of fluid extraction regulations (Preti et al., 2008; Marcaccio and Mazzei, 2023). The residuals, representing interannual variability not explained by the deterministic trend, were then modeled using two stochastic approaches: an Autoregressive Model of order 1 (AR(1)) and a Gauss–Markov (GM) process. Both methods account for short-term memory and autocorrelation by linking each

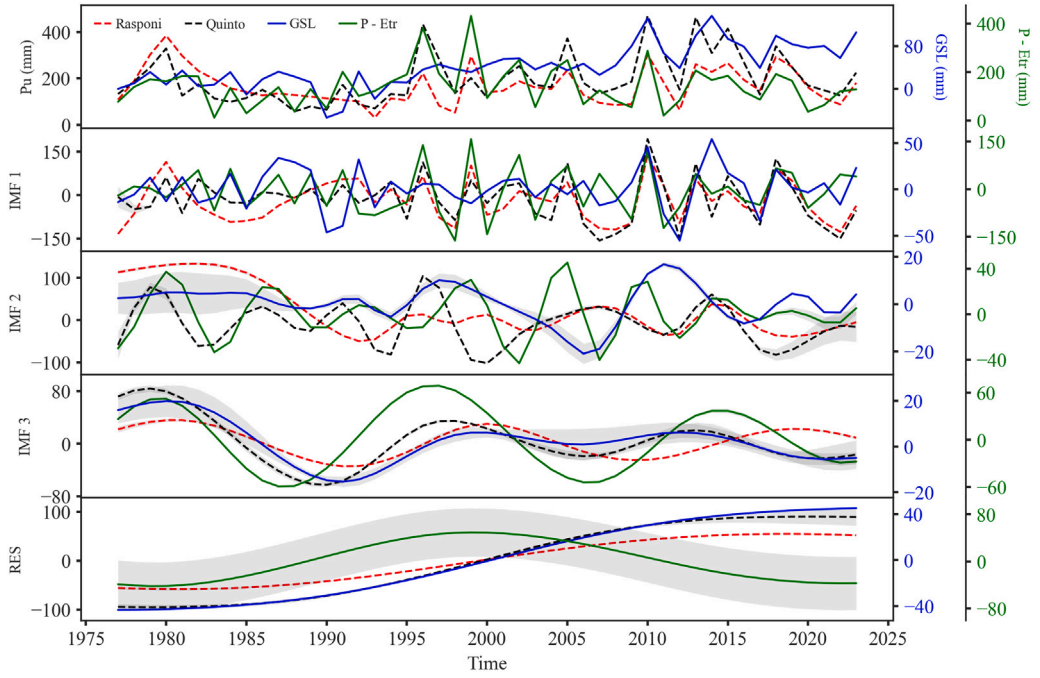

Fig. 4. Original time series (top panel) of P_u at Quinto (black dashed), P_u at Rasponi (red dashed), GSL (blue solid), and $P - Etr$ (green solid). Second, third, and fourth panels show the ensemble-mean IMFs 1, 2, and 3, respectively, for each variable, plotted in the same colors as the originals. The bottom panel shows the non-oscillatory residual trends of each series. The associated 1σ spread across the 1000 CEEMDAN realizations is indicated by the gray shading.

year's value to the previous one, with added Gaussian noise to simulate realistic temporal variability in VLM rates. These models were calibrated using the historical residuals and used to generate 1000 independent stochastic simulations each, projecting annual VLM rates from 2024 to 2100. Since a threshold of −2 mm/yr reflects the natural component of the VLM in the area (Gambolati et al., 1999; Carminati and Di Donato, 1999; Bitelli et al., 2000; Carminati and Martinelli, 2002; Antonellini et al., 2019), and may represent a realistic lower bound beyond which further deceleration is not expected to occur within this century, a constraint was imposed to ensure that the projected deterministic trend, once it reached −2 mm/yr, would remain constant for all subsequent years. Starting from the observed cumulative VLM value in 2023, future trajectories were computed by summing the simulated annual velocities. This process yielded 1000 cumulative VLM trajectories per model. For each projected year, the 10th, 50th, and 90th percentiles were computed from the ensemble of simulations (Fig. 3f).

3.3. Signal decomposition

The signal decomposition was carried out with the Complete Ensemble Empirical Mode Decomposition with Adaptive Noise (CEEMDAN) (Torres et al., 2011) applied to the annual P_u records of the Quinto and Rasponi basins, as well as to the $P - Etr$ and GSL series. CEEMDAN was executed 1000 times for each dataset, each run being initialized with an independent random-noise seed to minimize mode mixing. As an extensively improved evolution of the empirical-mode framework originally proposed by Huang et al. (1998), CEEMDAN offers a fully data-driven, scale-adaptive representation that is well-suited to non-parametric and non-stationary geophysical signals and has been widely adopted for denoising tasks in geoscience applications (Han and van der Baan, 2015; Jicheng et al., 2021; Meli, 2024; Yuan et al., 2023).

Each CEEMDAN realization produced a set of Intrinsic Mode Functions (IMFs). Due to the multiscale nature of environmental time series, individual IMFs may isolate dominant processes acting at local to regional scales, so that similar modes and long-term trends can be interpreted as manifestations of shared physical drivers (Ezer and Corlett, 2012). Each IMF obtained at the same order position across the 1000 repetitions was averaged, and their dispersion was quantified as the population standard deviation, thereby yielding an ensemble-mean IMF and its 1σ uncertainty envelope. For the present datasets, the CEEMDAN procedure returned four distinct modes of variability (see Fig. 4). IMF 1 captures interannual variability, IMF 2 isolates fluctuations on a near-decadal timescale, and IMF 3 resolves multidecadal variability. The fourth and final IMF is not oscillatory, and it corresponds to the residual trend (RES) of each series, which is interpreted as the long-term background evolution of the signal. The Hilbert transform, an entirely data-driven method making no distributional or linearity assumptions and commonly used to characterize the instantaneous periodicity of IMF modes, was applied to detect the periodicity of oscillatory modes.

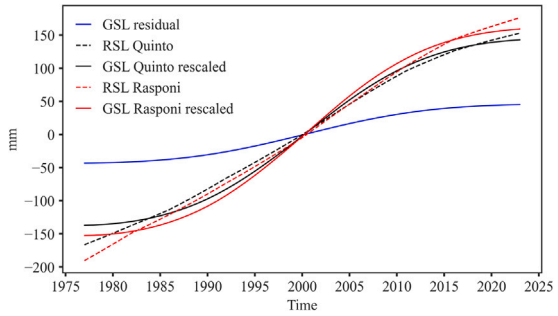

Fig. 5. RSL for the Quinto (black dashed line) and Rasponi (red dashed line) basins, computed using the classical formulation (i.e., $RSL = GSL - VLM$), where the blue line represents the residual GSL signal extracted from the decomposition, and VLM is the cumulative subsidence time series (shown in Fig. 3f). Solid black and red lines represent amplitude-rescaled versions of the residual GSL signal, adjusted to match the RSL variance, thereby incorporating the effect of local subsidence while preserving the shape of GSL evolution.

3.4. Multivariate dynamic regression

The multivariate analysis considered both the oscillatory components and the slowly varying trends obtained from the CEEMDAN decomposition described in Section 3.3. The oscillatory group was reconstructed by summing IMFs from 1 to 3 (Fig. 4). Although each IMF has a near-zero mean, their reassembly exposed a small yet statistically significant negative trend in the two P_u series, a drift (different in the two series) that does not appear in the corresponding reassembled oscillatory signals of GSL or $P - Etr$. Conversely, the trend group coincided with the CEEMDAN residuals.

The GSL was kept unaltered in the oscillatory group since VLM data do not provide any information about oscillatory variability, due to both its nature and being reconstructed from piece-wise linear trends. Conversely, for the GSL residual signal, accounting for cumulative VLM was necessary to reflect the full impact of RSL. However, the direct application of the classic relationship produced an unrealistic signal, as the VLM itself is not available as a consistent, annually resolved time series but is instead reconstructed from piece-wise linear trends (see Section 3.1). Thus, the GSL residual was amplitude-rescaled so that its variance matches the variance implied by the classic RSL formulation, given the available VLM trend estimates, while the temporal shape is preserved (Fig. 5). The rescaling multiplies every deviation from the GSL mean by the factor $\alpha = \sigma_{RSL}/\sigma_{GSL}$ and then restores the original mean. The resulting series retains the year-to-year pattern of the GSL residual while carrying the VLM-related variance implied by the classic formulation.

All signals were modeled without prior detrending, so that the full long-term relationship among P_u, sea-level terms, P, and Etr was retained. In the oscillatory block obtained from IMFs 1–3, the variables were labeled GSL_{osc} for the sea-level component; $P - Etr_{osc}$ for the hydroclimatic component; and Qui_{osc} and Ras_{osc} for the corresponding P_u series. In the residual trend block, conversely, the hydroclimatic term became $P - Etr_{res}$; the two P_u series were labeled Qui_{res} and Ras_{res}; and the GSL terms, here rescaled to account for the cumulative VLM of the two basins, were denoted RSL_{qui} (for Quinto) and RSL_{ras} (for Rasponi).

At this stage, each P_u record, Quinto or Rasponi, served as the endogenous series and was modeled with a state–space ARIMAX specification that combines an autoregressive term with two contemporaneous exogenous forcings, the sea-level signal and the hydroclimatic balance $P - Etr$, within a dynamic regression framework (Hamilton, 1994; Hyndman and Athanasopoulos, 2021)

$$y_t = \phi\, y_{t-1} + \beta_{\text{sea}}\, x_t^{(\text{sea})} + \beta_{\text{hyd}}\, x_t^{(\text{hyd})} + \varepsilon_t \qquad \varepsilon_t \sim \mathcal{N}(0, \sigma^2) \tag{4}$$

where y_t denotes the annual P_u at time t (either Qui_{osc} or Ras_{osc}) in the oscillatory group, and Qui_{res} or Ras_{res} in the residual group; $x_t^{(sea)}$ is the sea-level predictor (GSL_{osc} in the oscillatory analysis and RSL_{qui} or RSL_{ras} in the trend analysis); $x_t^{(hyd)}$ is the hydroclimatic predictor ($P - Etr_{osc}$ for the oscillatory fits and $P - Etr_{res}$ for the trend fits). The coefficient ϕ captures the year-to-year persistence of P_u, while β_{sea} and β_{hyd} quantify the contemporaneous response of P_u to a one-millimeter change in sea level and to a one-millimeter change in the hydroclimatic balance. At last, the term ε_t collects the unexplained variability and is assumed to be Gaussian white noise with variance σ^2.

The time series were subjected to the unit-root and co-integration tests that precede fitting the ARIMAX models (Engle and Granger, 1987; Hyndman and Athanasopoulos, 2021). For the oscillatory group, the augmented Dickey–Fuller test (Dickey and Fuller, 1981) always rejected the unit-root null at the 5% level, indicating that these signals are stationary in level. The residual group behaves differently, as all series failed the test and therefore appeared to be integrated of order one. However, regressing I(1) variables in levels is nonetheless admissible when they are co-integrated (Engle and Granger, 1987; Harris and Sollis, 2003). Then, a Johansen trace test (Johansen, 1991), applied to the three-variable system for each basin (constant term, one lag of differences), rejected the null hypothesis of no co-integration, so the residual signals can also be retained in levels. Consequently, all series were entered directly into the AR model with exogenous inputs, without differencing, and the slope coefficients retained the intuitive scale of millimeters of P_u per millimeter of forcing.

Since the oscillatory series were stationary and the residual series were co-integrated in levels, no differencing was required, and the series were therefore entered in levels for estimation. Normal-error assumptions held: residual skewness is always below 0.53,

and Jarque–Bera tests yield p-values of 0.52 (Quinto) and 0.31 (Rasponi), indicating negligible departures from normality (Jarque and Bera, 1980). Collinearity was minimal, as the variance-inflation factors achieved were under 2 (Neter et al., 1996), while Ljung–Box p-values above 0.40 showed that a single AR(1) term removes the remaining autocorrelation (Ljung and Box, 1978). Finally, an information-criterion search revealed that neither AIC nor BIC improved when extra AR or MA lags were introduced, so the most parsimonious and statistically adequate choice for both data blocks was an ARIMAX(1,0,0), i.e., an AR(1) model with contemporaneous sea-level and hydroclimatic exogenous inputs. The coefficients achieved were subsequently used to reconstruct, for each basin, the component of P_u that can be attributed deterministically to the exogenous forcings.

As dynamical systems depend on past information to forecast future states (Ljung, 2010), the achieved deterministic relationships were then combined with scenario projections (Section 3.2) to generate future P_u trajectories. In detail, the estimated coefficients from the ARIMAX models were applied to future projections of the exogenous variables under the SSP1-2.6, SSP2-4.5, SSP3-7.0, and SSP5-8.5 scenarios. For each scenario, the 10th, 50th, and 90th percentile trajectories were considered separately and consistently, such that the 10th percentile of each forcing was combined with the corresponding 10th percentile of the other, and likewise for the 50th and 90th percentiles. Since the sea-level projections are expressed in geocentric terms, they were adjusted to account for projected VLM (Fig. 3f) specific to each basin, following the rescaling procedure previously described.

4. Results

4.1. Environmental and hydroclimatic evolution

Time series from the two coastal pumping stations (Fig. 2) exhibit an overall rising trend, indicating a consistent increase in drainage requirements over time. However, this long-term rise is partially masked by a pronounced peak around 1980, which exerts strong leverage on trend estimates, followed by a decline that lasted until the early 1990s, with average P_u volumes dropping from over 200 mm to around 130 mm in both basins. Thereafter, volumes gradually increased, and in recent years, particularly at Quinto, have returned to levels comparable to those observed before the 1980s, or even higher. Once high-frequency components associated with interannual to multidecadal variability are removed, the residual signal (Fig. 4) reveals a similar nonlinear trend in both basins, with slight differences in magnitude.

The P time series (Fig. 3a) shows lower average values during the 1980s and early 1990s (approximately 570 mm), followed by a sharp increase in 1995–2010 (around 705 mm) and a modest decline in 2010–2023 (around 660 mm). Projections indicate little to no change under SSP1, slight decreases under SSP2 and SSP3, and a more pronounced drop under SSP5, though even SSP5 is not expected to return P to the low levels observed in the first part of the time series. Conversely, T (Fig. 3b) has risen steadily since the 1980s, from a mean of 12.6 °C in 1980–1995 to 13.6 °C in 1995–2010 and 15.1 °C in 2010–2023. Under SSP1, the warming is projected to slow after the 2050s, reaching about 16.2 °C by 2100, whereas SSP2, SSP3, and SSP5 all foresee continued warming, with median end-of-century T of roughly 17.5 °C, 18.8 °C, and 20.5 °C, respectively.

The Etr (Fig. 3c) increased steadily until the early 2000s and then stabilized. All scenario projections agree in extending this flattened behavior through to the end of the century. However, when P is combined with Etr in the water budget calculation (i.e., $P - Etr$ from Eq. (2)), the evolution of the time series differs. The balance increased until the late 1990s, then briefly stabilized before entering a declining trend (Fig. 3d), producing a well-defined convex shape in the $P - Etr$ residual signal (Fig. 4), and resulting in an overall variation ($\Delta P - Etr$) close to zero over time. Scenario SSP1 indicates a return to near-stable conditions after the 2040s, whereas the other pathways suggest a steady decline in $P - Etr$ through 2100. Because this balance quantifies the water available for surface runoff and for the pumping stations to drain, its projected decrease implies a progressively lower hydro-climatic load on the drainage system under SSP2, SSP3, and SSP5 scenarios.

Local annual GSL (Fig. 3e) shows a non-linear yet persistent rising trend, with rates varying depending on the period considered. Overall, during the 1977–2023 period, the observed increase, expressed as the net change of the residual signal, is approximately 89 mm. When GSL is variance-matched to RSL by rescaling (Fig. 5), its magnitude increases by about 218% at Quinto and 254% at Rasponi, due to local VLM. Modeled projections suggest the VLM will continue to decelerate, potentially approaching the natural threshold of –2 mm · yr^{-1} by the 2030s at Quinto and the 2040s at Rasponi. Consequently, future VLM impacts are expected to be smaller than in the past (see also Tables A1 and A2), with median cumulative displacements by 2100 (relative to 2024) of approximately –138 (–130, –145) mm at Quinto and –124 (–104, –140) mm at Rasponi (values in parentheses represent the 10th and 90th percentiles, respectively).

When considering only the residuals without the oscillatory components, the following observations emerge. From 1977 to 2023, annual P_u increased by 185 mm in the Quinto basin, and by 107 mm in the Rasponi basin, in agreement with Giambastiani et al. (2020). Over the same period, cumulative VLM reached approximately –231 mm at Quinto and –278 mm at Rasponi (Fig. 3f), while GSL rose by about 89 mm (Fig. 3e). As a result, RSL increased by 320 mm in the Quinto basin and 367 mm in the Rasponi basin. Based on the relationships defined in Eq. (3), the estimated increase in inflow over this time span is about 152 mm for Quinto and 175 mm for Rasponi (see also Tables A1 and A2). Thus, the discrepancy observed between the two basins yields different values: 33 mm in Quinto and –68 mm in Rasponi. When considered separately, over 1977–2023, VLM accounts for 72% of RSL at Quinto and 73% at Rasponi, while GSL accounts for the remaining 28% and 27%, respectively.

Finally, the oscillatory signals (Fig. 4) align with the physical interpretation of the CEEMDAN modes: interannual variability is captured by IMF-1 (periods of 2.8–4.2 years), near-decadal variability by IMF-2 (6–11.5 years), and multidecadal variability by IMF-3 (16.6–21 years). Once the oscillatory modes from the P_u signals have been reassembled (Fig. 6a), a significant negative trend emerges, showing that these near-zero-mean periodic components are not strictly stationary. Specifically, the reconstructed oscillations exhibit trends of –2.5 mm · yr^{-1} at Quinto and –3.3 mm · yr^{-1} at Rasponi. By contrast, the corresponding oscillatory components of GSL and $P - Etr$ remain stationary, with no detectable long-term drift.

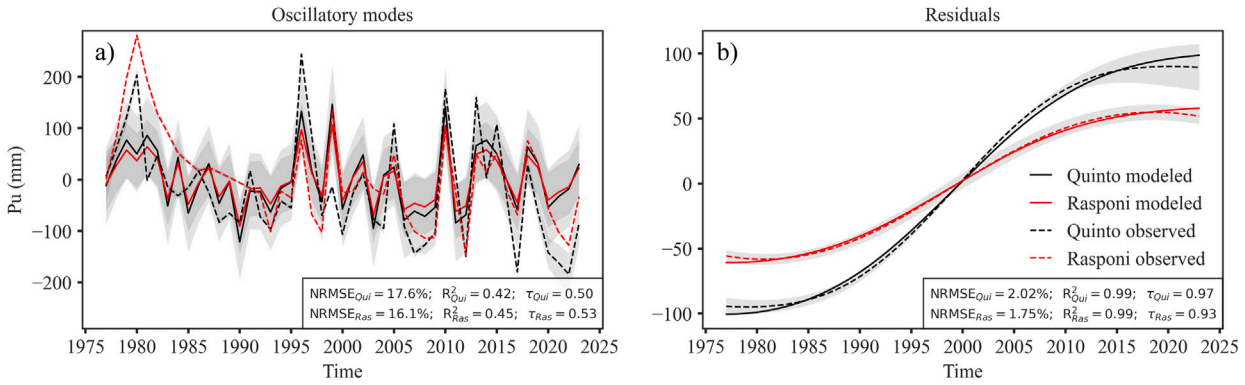

Fig. 6. Dashed lines show the reassembled oscillatory signals (a) and residual signals (b) for the Quinto (black) and Rasponi (red) P_u series. Solid lines show the series reconstructed by applying the model coefficients to the GSL and $P - Etr$ predictors. Gray shading indicates the 1σ spread across the 1000 CEEMDAN realizations. The legend in panel b also applies to panel a. In the bottom-right corner of each panel, the NRMSE, R^2, and Kendall's τ values are reported.

4.2. Model evaluation

The estimated parameters on the oscillatory signals indicate a substantial influence of both covariates in both basins. For Quinto, GSL shows a coefficient of 0.91, suggesting a strong, albeit marginally significant (p = 0.06), response to sea-level oscillations, while $P - Etr$ is highly significant ($p < 0.01$) with a coefficient value of 0.63, confirming a stable and relevant influence of hydroclimatic conditions. For Rasponi, both coefficients are statistically significant: 0.70 (p = 0.02) for GSL and 0.46 ($p < 0.01$) for $P - Etr$, indicating a significant contribution of the two drivers to the oscillatory dynamics, though with lower amplitude compared to Quinto. In both basins, model residuals are approximately normally distributed and show no significant autocorrelation, indicating adequate model specification despite the complexity of the signal.

Performance metrics for the oscillatory components (see also Fig. 6a) show comparable results across the two sites. For Quinto, the normalized root mean square error (NRMSE) is 17.6%, with an R^2 of 0.42 and a Kendall's τ of 0.50. For Rasponi, slightly better performance is observed, with an NRMSE of 16.1%, R^2 of 0.45, and Kendall's τ of 0.53, reflecting a marginally higher temporal consistency and variance explained by the model. Thus, an NRMSE below 20% is commonly considered indicative of good performance (Li et al., 2013), while an R^2 around 0.45 indicates that approximately half of the variance is explained by the model, and a Kendall's τ close to 0.5 suggests moderate agreement in the temporal ordering of observed and simulated values.

The model results on the CEEMDAN residuals reveal a strong and consistent influence of both covariates, particularly in the Quinto basin. RSL is highly significant ($p < 0.01$) with a coefficient of 0.71, and $P - Etr$ also shows a statistically significant association (p = 0.02) albeit with a weaker effect (coefficient = 0.08). For Rasponi, RSL remains the dominant driver ($p < 0.01$, coefficient = 0.38), while the contribution of $P - Etr$ is weak (0.07) and not statistically significant (p = 0.13). In contrast to the oscillatory case, both models exhibit extremely high autoregressive persistence, with AR(1) coefficients approaching unity in both basins (0.99), indicative of strong memory and smooth temporal evolution. Model residual diagnostics confirm that errors are well distributed, with approximate normality and no significant autocorrelation or heteroskedasticity. Model accuracy is considered excellent in both cases (Fig. 6b), with NRMSE of 2.02% for Quinto and 1.75% for Rasponi. R^2 values reach 0.99 for both basins, indicating near-total variance explained by the overall model in-sample, and Kendall's τ values of 0.97 (Quinto) and 0.93 (Rasponi) reflect a near-perfect temporal alignment between modeled and observed trends. Thus, this parameterization can reconstruct the slow residual evolution of both P_u time series with high accuracy.

4.3. Projection of pumping dynamics based on exogenous drivers

After applying the parameters estimated on the CEEMDAN residuals to the RSL and $P - Etr$ projections, deterministic scenario-based reconstructions of P_u dynamics were generated up to the year 2100 (Fig. 7). These reconstructions, based exclusively on low-frequency residual signals (i.e., long-term nonlinear trends in RSL and $P - Etr$), are referenced to a 2024 baseline and reflect only the slow cumulative evolution of P_u demands under different climate and sea-level scenarios. High-frequency variability is excluded due to the intrinsic unavailability of future oscillatory signals. Therefore, the scenario-based estimates represent the potential drainage requirement driven by the persistent and largely unavoidable influence of RSL rise, which accounts for the majority of the long-term signal (as shown in Section 4.2).

By 2050, relative to 2024 (also refer to Tables A1 and A2), the projected annual drainage requirement increase ranges from approximately +108 mm (in the most optimistic scenario) to +134 mm (in the worst) at Quinto, and from +55 to +68 mm at Rasponi, denoting minimal divergence by mid-century. The associated variability, derived from the most conservative 10th–90th percentile range across all scenarios, spans from +68 to +215 mm at Quinto and from +36 to +109 mm at Rasponi. In the same time frame and relative to the 2024 baseline, the VLM will add around 50 mm in the Quinto basin and approximately 40 mm in

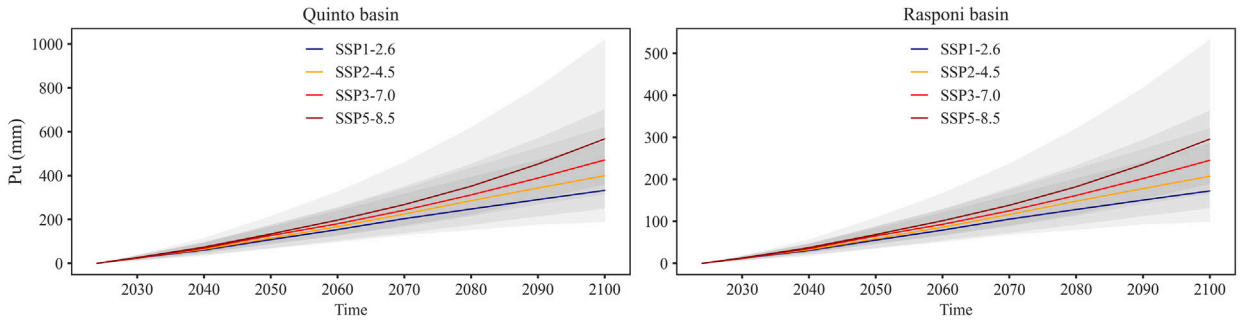

Fig. 7. Scenario-based reconstructions of the potential drainage requirement change over the period 2024–2100 for the Quinto (left panel) and Rasponi (right panel) basins. Projected values are referenced to the 2024 baseline and incorporate all four SSPs considered in this study. The magnitude of these projections reflects only the potential effect induced by the CEEMDAN residual trend signals of RSL and $P - Etr$.

the Rasponi basin, whereas the GSL by 2050 will increase from about 106 (SSP1) to 144 (SSP5) mm. According to these scenarios, expected local RSL will reach values around 150 to 190 mm in both basins. Over the period 2024–2050, for different scenarios, the contribution of VLM to RSL ranges from 25%–31% in the Quinto basin and 23%–28% in the Rasponi basin, while GSL accounts for 69%–75% and 72%–77%, respectively.

After 2050, scenario trajectories begin to diverge substantially. Indeed, by 2100 (with reference to 2024), projected increases in annual drainage requirements for the Quinto basin reach median values (with 10th and 90th percentiles in parentheses) of 332 (189, 554) mm for SSP1, 399 (250, 622) mm for SSP2, 471 (315, 703) mm for SSP3, and 567 (360, 1020) mm for SSP5. At Rasponi, the corresponding values are generally lower, with 172 (99, 286) mm for SSP1, 207 (131, 322) mm for SSP2, 245 (166, 364) mm for SSP3, and 296 (190, 532) mm for SSP5. Moreover, by 2100 the VLM term will add around 138 mm in the Quinto basin and 124 mm in the Rasponi basin, whereas the GSL, by 2100 for SSP1 and SSP5, will increase from 331 (122, 653) to 671 (369, 1321) mm. In this context, RSL will range from 469 to 809 mm in the Quinto basin and 455–795 mm in the Rasponi basin. By using the relationships in Eq. (3), inflow increases at the end of the century are estimated at 223–386 mm in the Quinto basin and 217–379 mm in the Rasponi basin. Over the 2024–2100 period, GSL remains the dominant driver of RSL, contributing 71%–83% at Quinto and 73%–84% at Rasponi.

Although projections based on long-term trends suggest a potentially substantial increase in drainage system requirements, short- to medium-term variability in GSL and $P - Etr$, while not directly projectable, may still significantly amplify or dampen cumulative trends. The trajectories shown in Fig. 7 should therefore be interpreted as potential baselines, to which periodic variability could be superimposed. Historical analysis of oscillatory components, reconstructed through CEEMDAN decomposition and modeled using ARIMAX, indicates that this variability might modulate the P_u signal by up to approximately ± 73 mm at Quinto and ± 55 mm at Rasponi (based on the 10th–90th percentile range). However, this modeled contribution explains only about half of the observed historical oscillatory signal (as discussed in Section 4.2). The remaining unexplained variability, not attributable to RSL and $P - Etr$, has a 10th–90th percentile range of approximately ± 113 mm at Quinto and ± 65 mm at Rasponi, likely reflecting additional unmodeled processes.

5. Discussion

The projections to the end of the century (Fig. 7) based on CEEMDAN residuals (Fig. 6b) represent only a portion of the potential future drainage requirements, as the future contribution of interannual to multidecadal oscillations (Fig. 6a) is intrinsically unavailable. However, the impact on drainage associated with the residuals, mainly explained by the RSL term (while the hydroclimatic driver contributes only marginally), is likely to be persistent and unavoidable, and is also well captured by the modeling. Indeed, the RSL term might be the driver of the S-shaped residuals observed in the P_u evolution of both basins (Figs. 4 and 6b). This shape reflects the widely reported acceleration of global and regional sea-level rise since the early 1990s, largely driven by warming-induced steric expansion (Cazenave et al., 2001). However, more recently, much of the Mediterranean Sea has experienced a deceleration in this trend, attributed to enhanced evaporation and salinization, with the associated mass loss and contraction of the water column, respectively (Meli et al., 2023; Borile et al., 2025). In the coming decades, sea-level rise is expected to accelerate globally, even if SSP1 mitigation targets are achieved, albeit with regional variations in magnitude (Fox-Kemper et al., 2021). This is primarily due to the delayed response of both ocean water warming and continental ice sheets/glaciers melting to environmental forcing, which will likely become the dominant driver of increasing drainage requirements toward 2100 (Fig. 7), assuming local VLM does not re-accelerate.

In addition to the persistent influence of the residuals in the coming decades, oscillations resulting from interannual to multidecadal variability (Fig. 4) periodically amplify or reduce drainage requirements. When reassembled (Fig. 6), the oscillatory term based on GSL and $P - Etr$ appears to fluctuate in phase with the P_u signal and shows a moderate explanatory capacity, with approximately 50% of the variability explained. These results suggest that, while the model accurately captures the residual trend component, the oscillatory variability remains more uncertain and may require additional variables or dedicated modeling

approaches for a more comprehensive explanation. To obtain a complete view of future potential requirements, the magnitude of the remaining unexplained oscillatory variability, likely attributable to a combination of physical, climatic, and anthropogenic factors not captured by RSL and $P - Etr$, should also be considered. These factors may include, for instance, effects induced by changes in land use and surface sealing, occasional or undocumented operational practices, and temporal changes in canal conveyance capacity or operational rules (Shang et al., 2025), all of which can affect the short-term variability of the drainage demand even if they have limited influence on long-term trends, as locally observed by Giambastiani et al. (2020).

Part of the unexplained variability may also reflect processes that operate at sub-annual scales and are not explicitly resolved by the annual aggregation adopted in this study. For instance, short-duration extreme events are also a plausible source of this unresolved component, whose timing and intensity are not directly captured by low-frequency signals and are absorbed by the unexplained oscillatory component. Indeed, a long-term decline in $P - Etr$ does not preclude increasing operational stress on the drainage system if precipitation becomes more intermittent and concentrated into heavy events, which can still contribute disproportionately to annual runoff totals and therefore to annual drainage volumes (Chang et al., 2023). Recent work has emphasized that the effect of climate change on extreme-value behavior depends strongly on the temporal resolution, with skewness typically larger at hourly than at daily/annual scales, and with potentially important implications for design quantiles and failure probability of hydraulic works (De Luca et al., 2024). In parallel, observational and attribution studies indicate increasing frequency of heavy precipitation extremes in many regions (Papalexiou and Montanari, 2019), while the probability of compound flooding has increased in some locations (Hsiao et al., 2021) and is expected to continue increasing with sea-level rise and intensifying heavy precipitation (IPCC, 2023). This compound-hazard framework is particularly relevant for coastal polders, where elevated sea levels can reduce drainage efficiency while intense rainfall loads the network over short time windows (Wahl et al., 2015).

Beyond extremes, changes in mean hydroclimatic conditions also matter, specifically changes in T and P, on coastal polder basins such as the Quinto and Rasponi basins, with particular attention to changes in P_u. As T rises due to climate change (Fig. 3b), Etr is also expected to increase. In principle, higher Etr could offset some of the effects of stable or even slightly increased P by reducing the volume of water reaching the drainage network. However, this relationship is not linear and depends on factors such as land use, vegetation type, soil moisture, and atmospheric conditions. In agricultural or wetland-dominated polders, such as the studied basins, the increase in Etr may be constrained by soil moisture availability. Once the soil dries out, Etr plateaus or declines, meaning that the net effect on the water balance could be marginal. This is consistent with the $P - Etr$ trend projected by the model by the end of the century (Fig. 3d). In both basins, the annual changes in $\Delta P - \Delta$Etr are not significant, showing decreasing variations from –14 (SSP1) to –92 (SSP5) mm/yr (Tables A1 and A2). Furthermore, increased T leads to reduced soil water content and may enhance upward capillary flux from saline or brackish groundwater, thereby increasing the volume of surface water that must be drained in coastal basins.

At the interannual scale, however, additional sources of variability beyond the long-term trends may exert considerable influence on drainage dynamics. Geomorphological and basin-related characteristics, variations in shallow groundwater tables, or spatial heterogeneity in VLM rates (here assumed to be homogeneous across the basins), may also play a role. These same factors may contribute to the negative trends observed in the reassembled P_u oscillatory signals, suggesting that part of the oscillatory variability carries a persistent downward drift. This may result from unresolved low-frequency components due to imperfect mode separation but may also reflect internal system dynamics that have systematically reduced P_u demand over time. This is also suggested by the difference between the two observed negative trends, which might indeed be linked to internal differences between the basins. In terms of temporal evolution, the lack of a significant local P trend over the last decades (Crespi et al., 2018; Pavan et al., 2019; Meli and Romagnoli, 2022) does not explain the negative trends. Conversely, the strong increase in T since the 1980s, as also reported by Antolini et al. (2016) and Meli and Romagnoli (2022), might have led to a decrease in P_u requirements. However, the combined effect of such parameters, as observed through Etr, also suggests a lack of significance in terms of the residual trend, a pattern shown in the reassembled oscillations and already documented by Giambastiani et al. (2020). The negative trends observed could simply be related to the limited length of the available P_u data, as the first part of the oscillatory terms is characterized by a strong positive peak, while the final part shows a strong negative peak, leading to negative trends due to edge effects. The positive peak was the last of a series of intense pumping events, driven by several concurrent factors such as the exceptionally high VLM before the 1980s (Gambolati et al., 1991) and the gradual reclamation of residual brackish wetlands and marshes during the 1970s (Bondesan et al., 1978; Bruno et al., 2024). Thus, the negative trends embedded within the reassembled oscillatory signals reflect only the 1977–2023 evolution and may diminish or even reverse in the coming decades.

An interesting aspect lies in the fact that the modeled parameters for both P_u residual trends and oscillatory variability show a stronger relationship with sea-level terms, whereas $P - Etr$, despite being highly significant within the oscillatory terms, yields weaker correlations. At the same time, values observed for Quinto are higher than those from Rasponi for both trends and oscillatory terms. The only differing signal considered between the two basins is local VLM, as GSL and $P - Etr$ are shared. However, despite being slightly stronger in magnitude at Rasponi, the temporal evolution of VLM is similar in both basins and cannot explain the discrepancies in the modeled parameters. Moreover, the oscillatory signals do not account for VLM, as only GSL is considered in this case. Therefore, this difference may be attributed to other factors internal to the basin dynamics. The attenuated trends observed at Rasponi, compared to the Quinto basin, could be related to a lower hydraulic conductivity of the Rasponi aquifer and to the presence of more open water surface areas (quarry lakes and wetlands) in Quinto than in Rasponi.

Examination of Tables A1 and A2 reveals that, according to future projections, the relative contributions of VLM and GSL to the increase in P_u are expected to shift significantly, with GSL gaining increasing importance. By 2100 (relative to 2024), GSL is projected to account for approximately 70% to over 80% of the RSL, depending on the scenario. In contrast, the contribution of local VLM is expected to decrease to less than 20% in both basins. The discrepancies between the CEEMDAN-based projections

and the estimates obtained using Eq. (3) can be attributed to minor offsets related to changes in $\Delta P - \Delta \mathrm{Etr}$. In the Rasponi basin, however, the differences in absolute value are more substantial (see Tables A1 and A2, column $|\Delta P_u - \Delta Q_v|$). These discrepancies are substantially reduced when assuming a hydraulic conductivity of K = 0.02 m/d instead of 0.03 m/d, suggesting that slight differences in the hydraulic properties of the aquifer beneath the Rasponi basin may explain the mismatch.

6. Conclusions

This study provides a comprehensive, data-driven assessment of long-term drainage dynamics in two coastal polder basins in the Ravenna territory (northeastern Italy), integrating nearly 50 years of historical records with advanced signal decomposition, dynamic regression modeling, and climate scenario projections. Results show that relative sea-level rise, driven by both local subsidence and geocentric sea-level change, has become the dominant factor influencing long-term pumping trends. While subsidence was historically the main forcing mechanism, its contribution is projected to decline due to deceleration trends, whereas sea-level rise is expected to accelerate, particularly under high-emission scenarios. This shift underscores the urgency for forward-looking water management strategies.

In the coming decades, energy demand for operating the drainage infrastructure is likely to increase, not only due to relative sea-level rise, which changes the hydraulic gradient and increases the seepage, but also because more energy may be required per unit of drained water. Moreover, interannual to multidecadal fluctuations will add variability to this demand, calling for more flexible and adaptive infrastructure planning. These evolving conditions point to the need for a shift in management priorities in the coastal polder basins of the Adriatic region. Whereas past management focused on coping with local land subsidence, future strategies must increasingly respond to global sea-level rise. Water managers and policymakers will therefore need to adopt new perspectives and develop long-term mitigation and adaptation measures. The proposed methodological framework is transferable to other polder basins worldwide, provided that comparable long-term time series are available. By supporting integrated coastal zone and water management, it can inform anticipatory adaptation strategies that consider both present trends and future scenarios.

CRediT authorship contribution statement

Matteo Meli: Writing – original draft, Visualization, Methodology, Investigation, Formal analysis. **Marco Antonellini:** Writing – review & editing, Writing – original draft, Supervision, Investigation. **Beatrice Maria Sole Giambastiani:** Writing – review & editing, Writing – original draft, Visualization, Investigation, Data curation, Conceptualization.

Declaration of competing interest

The authors declare that they have no known competing financial interests or personal relationships that could have appeared to influence the work reported in this paper.

Acknowledgments

The authors would like to thank Mario Molducci from the local Land Reclamation Consortium (Consorzio di Bonifica della Romagna) for providing drainage data and technical information on drainage operations, and Prof. Claudia Romagnoli and Prof. Sonia Silvestri for their support in securing the funding for this research. The authors also thank two anonymous reviewers for their constructive comments, which helped improve an early version of the manuscript. This study was carried out within the RETURN Extended Partnership and received funding from the European Union Next-GenerationEU (National Recovery and Resilience Plan – NRRP, Mission 4, Component 2, Investment 1.3 – D.D. 1243 2/8/2022, PE0000005).

Appendix

See Tables A1 and A2.

Data availability

Daily local precipitation and air temperature data for the period 1977–2023 were obtained from https://simc.arpae.it/dext3r/. Local geocentric sea-level time series (1993–2020) and subsidence estimates (2006–2021) were sourced from Meli et al. (2025), available at https://doi.org/10.5281/zenodo.14671018. Subsidence trends for 1977–1992 were derived from Teatini et al. (2005), while estimates for 1992–2006 were obtained from https://servizi-gis.arpae.it/Html5Viewer/index.html?locale=it-IT&viewer&viewer=Geoportal.Geoportal. Annual climate projections of local rainfall and mean surface temperature were retrieved from https://climateknowledgeportal.worldbank.org/country/italy/climate-data-projections, and sea-level projections from https://sealevel.nasa.gov/data_tools/17.

Table A1
Observed (1977–2023) and projected (2024–2050 and 2024-2100) values for parameters within the Quinto basin. Projection estimates differ according to the scenario considered (SSP1, SSP2, SSP3, and SSP5). For each column, the reported value corresponds to the 50th percentile, while the subscript values in parentheses indicate the 10th and 90th percentiles. For historical ΔP_u, as with ΔGSL and $\Delta P - \Delta E_{tr}$, values are derived from the non-linear RES trend extracted via decomposition (Fig. 4), since interannual to multidecadal variability and oscillations would otherwise render Δ estimates highly sensitive to the selected period. ΔVLM is non-climatic and therefore unaffected by emission scenarios, while ΔGSL and $\Delta P - \Delta E_{tr}$ are considered identical across both basins. Note that while ΔVLM values are listed as positive, they indicate land subsidence (i.e., land lowering). Eq. (3) is used to calculate ΔQ_v as an approximation of the seepage in polder basins with a phreatic aquifer (Vlotman et al., 2020). Discrepancy, in absolute terms, refers to the difference between ΔP_u and ΔQ_v. The last two columns represent the percentage contribution of ΔVLM and ΔGSL to ΔRSL.

Period	Scenario	ΔP_u (mm)	ΔVLM (mm)	ΔGSL (mm)	ΔRSL (mm)	ΔQ_v (mm/yr)	$\lvert\Delta P_u - \Delta Q_v\rvert$ (mm/yr)	$\Delta P - \Delta Etr$ (mm/yr)	$\frac{\Delta VLM}{\Delta RSL}$ (%)	$\frac{\Delta GSL}{\Delta RSL}$ (%)
1977–2023		185	231	89	320	152	33	2	72	28
2024–2050	SSP1	$108_{(68,167)}$	$48_{(43,51)}$	$106_{(47,194)}$	$154_{(91,245)}$	$73_{(43,117)}$	$35_{(25,50)}$	$-16_{(-14,-23)}$	$31_{(47,21)}$	$69_{(52,79)}$
2024–2100	SSP1	$332_{(189,554)}$	$138_{(130,145)}$	$331_{(122,653)}$	$469_{(255,798)}$	$223_{(122,380)}$	$109_{(67,174)}$	$-14_{(-11,-24)}$	$29_{(51,18)}$	$71_{(48,82)}$
2024–2050	SSP2	$115_{(69,174)}$	$48_{(43,51)}$	$116_{(46,204)}$	$164_{(89,255)}$	$78_{(42,122)}$	$37_{(27,52)}$	$-18_{(-7,-19)}$	$29_{(48,20)}$	$71_{(52,80)}$
2024–2100	SSP2	$399_{(250,622)}$	$138_{(130,145)}$	$429_{(210,752)}$	$567_{(340,897)}$	$270_{(162,427)}$	$129_{(88,195)}$	$-42_{(-21,-52)}$	$24_{(38,16)}$	$76_{(62,84)}$
2024–2050	SSP3	$127_{(90,177)}$	$48_{(43,51)}$	$133_{(77,210)}$	$181_{(120,261)}$	$86_{(57,124)}$	$41_{(33,53)}$	$-20_{(-12,-34)}$	$27_{(36,20)}$	$73_{(64,80)}$
2024–2100	SSP3	$471_{(315,703)}$	$138_{(130,145)}$	$532_{(303,872)}$	$670_{(433,1017)}$	$319_{(206,485)}$	$152_{(109,218)}$	$-60_{(-38,-101)}$	$21_{(30,14)}$	$79_{(70,86)}$
2024–2050	SSP5	$134_{(87,215)}$	$48_{(43,51)}$	$144_{(75,266)}$	$192_{(118,317)}$	$92_{(56,151)}$	$42_{(31,64)}$	$-33_{(-24,-51)}$	$25_{(36,16)}$	$75_{(64,84)}$
2024–2100	SSP5	$567_{(360,1020)}$	$138_{(130,145)}$	$671_{(369,1321)}$	$809_{(499,1690)}$	$386_{(238,805)}$	$181_{(122,215)}$	$-92_{(-54,-129)}$	$17_{(26,9)}$	$83_{(74,91)}$

Table A2
Same as Table A1 but referring to the Rasponi basin.

Period	Scenario	ΔP_u (mm)	ΔVLM (mm)	ΔGSL (mm)	ΔRSL (mm)	ΔQ_v (mm/yr)	$\lvert\Delta P_u - \Delta Q_v\rvert$ (mm/yr)	$\Delta P - \Delta Etr$ (mm/yr)	$\frac{\Delta VLM}{\Delta RSL}$ (%)	$\frac{\Delta GSL}{\Delta RSL}$ (%)
1977–2023		107	278	89	367	175	68	2	76	24
2024–2050	SSP1	$55_{(36,84)}$	$42_{(30,50)}$	$106_{(47,194)}$	$148_{(77,244)}$	$71_{(37,69)}$	$16_{(1,15)}$	$-16_{(-14,-23)}$	$28_{(39,35)}$	$72_{(61,65)}$
2024–2100	SSP1	$172_{(99,286)}$	$124_{(104,140)}$	$331_{(122,653)}$	$455_{(226,793)}$	$217_{(108,378)}$	$45_{(9,92)}$	$-14_{(-11,-24)}$	$27_{(46,18)}$	$73_{(54,82)}$
2024–2050	SSP2	$59_{(36,88)}$	$42_{(30,50)}$	$116_{(46,204)}$	$158_{(76,254)}$	$75_{(36,121)}$	$16_{(0,33)}$	$-18_{(-7,-19)}$	$27_{(39,20)}$	$73_{(61,80)}$
2024–2100	SSP2	$207_{(131,322)}$	$124_{(104,140)}$	$429_{(210,752)}$	$553_{(314,892)}$	$264_{(150,425)}$	$57_{(19,103)}$	$-42_{(-21,-52)}$	$23_{(33,16)}$	$77_{(67,84)}$
2024–2050	SSP3	$65_{(47,89)}$	$42_{(30,50)}$	$133_{(77,210)}$	$175_{(107,260)}$	$84_{(51,124)}$	$19_{(4,35)}$	$-20_{(-12,-34)}$	$24_{(28,19)}$	$76_{(72,81)}$
2024–2100	SSP3	$245_{(166,364)}$	$124_{(104,140)}$	$532_{(303,872)}$	$656_{(407,1012)}$	$313_{(194,482)}$	$68_{(28,118)}$	$-60_{(-38,-101)}$	$19_{(26,14)}$	$81_{(74,86)}$
2024–2050	SSP5	$68_{(46,109)}$	$42_{(30,50)}$	$144_{(75,266)}$	$186_{(105,316)}$	$89_{(50,151)}$	$21_{(4,42)}$	$-33_{(-24,-51)}$	$23_{(29,16)}$	$77_{(71,84)}$
2024–2100	SSP5	$296_{(190,532)}$	$124_{(104,140)}$	$671_{(369,1321)}$	$795_{(473,1461)}$	$379_{(225,696)}$	$83_{(35,164)}$	$-92_{(-54,-129)}$	$16_{(22,10)}$	$84_{(78,90)}$

References

Akaike, H., 1974. A new look at the statistical model identification. IEEE Trans. Autom. Control 19 (6), 716–723. http://dx.doi.org/10.1109/TAC.1974.1100705.

Alexandrakis, G., Manasakis, C., Kampanis, N.A., 2015. Valuating the effects of beach erosion to tourism revenue. A management perspective. Ocean & Coastal Management 111, 1–11. http://dx.doi.org/10.1016/j.ocecoaman.2015.04.001.

Alifu, H., Hirabayashi, Y., Imada, Y., Shiogama, H., 2022. Enhancement of river flooding due to global warming. Sci. Rep. 12, 20687. http://dx.doi.org/10.1038/s41598-022-25182-6.

Antolini, G., Auteri, L., Pavan, V., Tomei, F., Tomozeiu, R., Marletto, V., 2016. A daily high-resolution gridded climatic data set for Emilia-Romagna, Italy, during 1961–2010. Int. J. Climatol. 36 (4), 1970–1986. http://dx.doi.org/10.1002/joc.4473.

Antonellini, M., Giambastiani, B.M.S., Greggio, N., Bonzi, L., Calabrese, L., Luciani, P., Perini, L., Severi, P., 2019. Processes governing natural land subsidence in the shallow coastal aquifer of the Ravenna coast, Italy. Catena 172, 76–86. http://dx.doi.org/10.1016/j.catena.2018.08.019.

Antonellini, M., Mollema, P., Giambastiani, B.M.S., Banzola, E., Bishop, K., Caruso, L., Minchio, A., Pellegrini, L., Sabia, M., Ulazzi, E., Gabbianelli, G., 2008. Salt water intrusion in The Coastal aquifer of the southern po-plain, Italy. Hydrogeol. J. 16, 1541–1556. http://dx.doi.org/10.1007/s10040-008-0319-9.

Bitelli, G., Bonsignore, F., Pellegrino, I., Vittuari, L., 2015. Evolution of the techniques for subsidence monitoring at regional scale: the case of Emilia-Romagna region (Italy). Proc. Int. Assoc. Hydrol. Sci. 372, 315–321. http://dx.doi.org/10.5194/piahs-372-315-2015.

Bitelli, G., Bonsignore, F., Unguendoli, M., 2000. Levelling and GPS networks to monitor ground subsidence in the Southern Po Valley. J. Geodyn. 30 (3), 355–369. http://dx.doi.org/10.1016/S0264-3707(99)00071-X.

Bondesan, M., Calderoni, G., Dal Cin, R., 1978. Il litorale delle province di Ferrara e di Ravenna (Alto Adriatico); evoluzione morfologica e distribuzione dei sedimenti. Ital. J. Geosci. 97 (3), 247–287.

Borile, F., Pinardi, N., Lyubartsev, V., Ghani, M.H., Navarra, A., Alessandri, J., Clementi, E., Coppini, G., Mentaschi, L., Verri, G., da Costa, V.S., Scoccimarro, E., Misurale, F., Novellino, A., Oddo, P., 2025. The Eastern Mediterranean sea mean sea level decadal slowdown: the effects of the water budget. Front. Clim. 7, http://dx.doi.org/10.3389/fclim.2025.1472731.

Bruno, L., Meli, M., Garberi, M.L., 2024. Human–induced landscape modification in the in the last two centuries in the po delta plain (northern Italy). Anthropocene 48, 100453. http://dx.doi.org/10.1016/j.ancene.2024.100453.

Campo, B., Amorosi, A., Vaiani, S.C., 2017. Sequence stratigraphy and late quaternary paleoenvironmental evolution of the Northern Adriatic coastal plain (Italy). Palaeogeogr. Palaeoclimatol. Palaeoecol. 466, 265–278. http://dx.doi.org/10.1016/j.palaeo.2016.11.016.

Carminati, E., Di Donato, G., 1999. Separating natural and anthropogenic vertical movements in fast subsiding areas: The po plain (N. Italy) case. Geophys. Res. Lett. 26 (15), 2291–2294. http://dx.doi.org/10.1029/1999GL900518.

Carminati, E., Martinelli, G., 2002. Subsidence rates in the po plain, northern Italy: the relative impact of natural and anthropogenic causation. Eng. Geol. 66 (3), 241–255. http://dx.doi.org/10.1016/S0013-7952(02)00031-5.

Cazenave, A., Cabanes, C., Dominh, K., Mangiarotti, S., 2001. Recent sea level change in the Mediterranean Sea revealed by Topex/Poseidon satellite altimetry. Geophys. Res. Lett. 28 (8), 1607–1610. http://dx.doi.org/10.1029/2000GL012628.

Chang, D., Li, S., Lai, Z., 2023. Effects of extreme precipitation intensity and duration on the runoff and nutrient yields. J. Hydrol. 626, 130281. http://dx.doi.org/10.1016/j.jhydrol.2023.130281.
Ciavola, P., Armaroli, C., Chiggiato, J., Valentini, A., Deserti, M., Perini, L., Luciani, P., 2007. Impact of storms along the coastline of Emilia-Romagna: the morphological signature on the Ravenna coastline (Italy). J. Coast. Res. 50 (sp1), 540. http://dx.doi.org/10.2112/JCR-SI50-103.1.
Cremonini, L., Randi, P., Fazzini, M., Nardino, M., Rossi, F., Georgiadis, T., 2024. Causes and impacts of flood events in Emilia-Romagna (Italy) in May 2023. Land 13 (11), http://dx.doi.org/10.3390/land13111800.
Crespi, A., Brunetti, M., Lentini, G., Maugeri, M., 2018. 1961–1990 high-resolution monthly precipitation climatologies for Italy. Int. J. Climatol. 38 (2), 878–895. http://dx.doi.org/10.1002/joc.5217.
Da Lio, C., Tosi, L., 2019. Vulnerability to relative sea-level rise in the po river delta (Italy). Estuar. Coast. Shelf Sci. 228, 106379. http://dx.doi.org/10.1016/j.ecss.2019.106379.
de Louw, P.G.B., van der Velde, Y., van der Zee, S.E.A.T.M., 2011. Quantifying water and salt fluxes in a lowland polder catchment dominated by boil seepage: a probabilistic end-member mixing approach. Hydrol. Earth Syst. Sci. 15 (7), 2101–2117. http://dx.doi.org/10.5194/hess-15-2101-2011.
De Luca, D.L., Ridolfi, E., Russo, F., Moccia, B., Napolitano, F., 2024. Climate change effects on rainfall extreme value distribution: the role of skewness. J. Hydrol. 634, 130958. http://dx.doi.org/10.1016/j.jhydrol.2024.130958.
Dickey, D.A., Fuller, W.A., 1981. Likelihood ratio statistics for autoregressive time series with a unit root. Econometrica 49 (4), 1057–1072. http://dx.doi.org/10.2307/1912517.
Engle, R.F., Granger, C.W.J., 1987. Co-integration and error correction: Representation, estimation, and testing. Econometrica 55 (2), 251–276. http://dx.doi.org/10.2307/1913236.
Ezer, T., Corlett, W.B., 2012. Is sea level rise accelerating in the Chesapeake Bay? A demonstration of a novel new approach for analyzing sea level data. Geophys. Res. Lett. 39 (19), http://dx.doi.org/10.1029/2012GL053435.
Farrell, W.E., Clark, J.A., 1976. On postglacial sea level. Geophys. J. Int. 46 (3), 647–667. http://dx.doi.org/10.1111/j.1365-246X.1976.tb01252.x.
Fiaschi, S., Tessitore, S., Bonì, R., Di Martire, D., Achilli, V., Borgstrom, S., Ibrahim, A., Floris, M., Meisina, C., Ramondini, M., Calcaterra, D., 2017. From ERS-1/2 to sentinel-1: two decades of subsidence monitored through A-DInSAR techniques in the ravenna area (Italy). GIScience Remote. Sens. 54 (3), 305–328. http://dx.doi.org/10.1080/15481603.2016.1269404.
Fox-Kemper, B., Hewitt, H.T., Xiao, C., Aðalgeirsdóttir, G., Drijfhout, S.S., Edwards, T.L., Golledge, N.R., Hemer, M., Kopp, R.E., Krinner, G., Mix, A., Notz, D., Nowicki, S., Nurhati, I.S., Ruiz, L., Sallée, J.-B., Slangen, A.B.A., Yu, Y., 2021. Ocean, cryosphere and sea level change. In: Masson-Delmotte, V., Zhai, P., Pirani, A., Connors, S.L., Péan, C., Berger, S., Caud, N., Chen, Y., Goldfarb, L., Gomis, M.I., Huang, M., Leitzell, K., Lonnoy, E., Matthews, J.B.R., Maycock, T.K., Waterfield, T., Yelekçi, O., Yu, R., Zhou, B. (Eds.), Climate Change 2021: The Physical Science Basis. Contribution of Working Group I to the Sixth Assessment Report of the Intergovernmental Panel on Climate Change. Cambridge University Press, Cambridge, United Kingdom and New York, NY, USA, pp. 1211–1362. http://dx.doi.org/10.1017/9781009157896.011.
Gambolati, G., Ricceri, G., Bertoni, W., Brighenti, G., Vuillermin, E., 1991. Mathematical simulation of the subsidence of Ravenna. Water Resour. Res. 27 (11), 2899–2918. http://dx.doi.org/10.1029/91WR01567.
Gambolati, G., Teatini, P., Tomasi, L., Gonella, M., 1999. Coastline regression of the Romagna region, Italy, due to natural and anthropogenic land subsidence and sea level rise. Water Resour. Res. 35 (1), 163–184. http://dx.doi.org/10.1029/1998WR900031.
Giambastiani, B.M.S., Kidanemariam, A., Dagnew, A., Antonellini, M., 2021. Evolution of salinity and water table level of the Phreatic Coastal aquifer of the Emilia Romagna Region (Italy). Water 13 (3), http://dx.doi.org/10.3390/w13030372.
Giambastiani, B.M.S., Macciocca, V.R., Molducci, M., Antonellini, M., 2020. Factors affecting water drainage long-time series in the salinized low-Lying Coastal area of ravenna (Italy). Water 12 (1), http://dx.doi.org/10.3390/w12010256.
Greggio, N., Mollema, P., Antonellini, M., Gabbianelli, G., 2012. Irrigation management in coastal zones to prevent soil and groundwater salinization. In: Abrol, V., Sharma, P. (Eds.), Resource Management for Sustainable Agriculture. IntechOpen, Rijeka, p. 308. http://dx.doi.org/10.5772/50534.
Gregory, J.M., Griffies, S.M., Hughes, C.W., Lowe, J.A., Church, J.A., Fukimori, I., Gomez, N., Kopp, R., Landered, F., Cozannet, G.L., Ponte, R.M., Stammer, D., Tamisiea, M.E., van de Wal, R.S.W., 2019. Concepts and terminology for sea level: Mean, variability and change, both local and global. Surv. Geophys. 40, 1251–1289. http://dx.doi.org/10.1007/s10712-019-09525-z.
Gudulas, K., Voudouris, K., Soulios, G., Dimopoulos, G., 2013. Comparison of different methods to estimate actual evapotranspiration and hydrologic balance. Desalination Water Treat. 51 (13), 2945–2954. http://dx.doi.org/10.1080/19443994.2012.748443.
Habel, S., Fletcher, C.H., Anderson, T.R., Thompson, P.R., 2020. Sea-level rise induced multi-mechanism flooding and contribution to urban infrastructure failure. Sci. Rep. 10, 3796. http://dx.doi.org/10.1038/s41598-020-60762-4.
Hamilton, J.D., 1994. Time Series Analysis. Princeton University Press, Princeton, New Jersey, USA.
Han, J., van der Baan, M., 2015. Microseismic and seismic denoising via ensemble empirical mode decomposition and adaptive thresholding. Geophysics 80 (6), KS69–KS80. http://dx.doi.org/10.1190/geo2014-0423.1.
Harris, R., Sollis, R., 2003. Applied Time Series Modelling and Forecasting. John Wiley & Sons.
Hsiao, S.-C., Chiang, W.-S., Jang, J.-H., Wu, H.-L., Lu, W.-S., Chen, W.-B., Wu, Y.-T., 2021. Flood risk influenced by the compound effect of storm surge and rainfall under climate change for low-lying coastal areas. Sci. Total Environ. 764, 144439. http://dx.doi.org/10.1016/j.scitotenv.2020.144439.
Huang, N.E., Shen, Z., Long, S.R., Wu, M.C., Shih, H.H., Zheng, Q., Yen, N.-C., Tung, C.C., Liu, H.H., 1998. The empirical mode decomposition and the Hilbert spectrum for nonlinear and non-stationary time series analysis. Proc. R. Soc. Lond. Ser. A Math. Phys. Eng. Sci. 454 (1971), 903–995. http://dx.doi.org/10.1098/rspa.1998.0193.
Hyndman, R.J., Athanasopoulos, G., 2021. Forecasting: Principles and Practice, third ed. OTexts, Melbourne, Australia.
IPCC, 2023. Future global climate: Scenario-based projections and near-term information. In: Climate Change 2021 – the Physical Science Basis: Working Group I Contribution to the Sixth Assessment Report of the Intergovernmental Panel on Climate Change. Cambridge University Press, Cambridge, United Kingdom and New York, NY, USA, pp. 553–672. http://dx.doi.org/10.1017/9781009157896.
Jarque, C.M., Bera, A.K., 1980. Efficient tests for normality, homoscedasticity and serial independence of regression residuals. Econom. Lett. 6 (3), 255–259. http://dx.doi.org/10.1016/0165-1765(80)90024-5.
Jicheng, L., Gu, Y., Chou, Y., and, J.G., 2021. Seismic data random noise reduction using a method based on improved complementary ensemble EMD and adaptive interval threshold. Explor. Geophys. 52 (2), 137–149. http://dx.doi.org/10.1080/08123985.2020.1777849.
Johansen, S., 1991. Estimation and hypothesis testing of cointegration vectors in Gaussian vector autoregressive models. Econometrica 59 (6), 1551–1580. http://dx.doi.org/10.2307/2938278.
Li, M.-F., Tang, X.-P., Wu, W., Liu, H.-B., 2013. General models for estimating daily global solar radiation for different solar radiation zones in mainland China. Energy Convers. Manage. 70, 139–148. http://dx.doi.org/10.1016/j.enconman.2013.03.004.
Ljung, L., 2010. Perspectives on system identification. Annu. Rev. Control. 34 (1), 1–12. http://dx.doi.org/10.1016/j.arcontrol.2009.12.001.
Ljung, G.M., Box, G.E.P., 1978. On a measure of lack of fit in time series models. Biometrika 65 (2), 297–303. http://dx.doi.org/10.2307/2335207.
Luo, J., Straffelini, E., Bozzolan, M., Zheng, Z., Tarolli, P., 2024. Saltwater intrusion in the po River Delta (Italy) during drought conditions: Analyzing its spatio-temporal evolution and potential impact on agriculture. Int. Soil Water Conserv. Res. 12 (3), 714–725. http://dx.doi.org/10.1016/j.iswcr.2023.09.009.
Maicu, F., De Pascalis, F., Ferrarin, C., Umgiesser, G., 2018. Hydrodynamics of the po river-delta-sea system. J. Geophys. Res.: Ocean. 123 (9), 6349–6372. http://dx.doi.org/10.1029/2017JC013601.

Marcaccio, M., Mazzei, M., 2023. Monitoraggio dei movimenti verticali del suolo e aggiornamento della cartografia di subsidenza nella pianura dell'Emilia–Romagna. Periodo 2016–2021. Technical Report, Regione Emilia–Romagna, Arpae Emilia–Romagna, Bologna, Italy, https://www.arpae.it/it/temi-ambientali/suolo/rapporti/rapporti-subsidenza/monitoraggio-movimenti-verticali-suolo-e-cartografia-subsidenza-emilia-romagna-2016-2021.zip/view. (In Italian).

Meli, M., 2024. The potential recording of North Ionian Gyre's reversals as a decadal signal in sea level during the instrumental period. Sci. Rep. 14, 4907. http://dx.doi.org/10.1038/s41598-024-55579-4.

Meli, M., Camargo, C.M.L., Olivieri, M., Slangen, A.B.A., Romagnoli, C., 2023. Sea–level trend variability in the Mediterranean during the 1993–2019 period. Front. Mar. Sci. 10, 1150488. http://dx.doi.org/10.3389/fmars.2023.1150488.

Meli, M., Marcaccio, M., Mazzei, M., Romagnoli, C., 2025. Temporal and spatial analysis of relative sea-level changes across the Emilia-Romagna coastal plain (northern Adriatic Sea). Estuar. Coast. Shelf Sci. 314, 109143. http://dx.doi.org/10.1016/j.ecss.2025.109143.

Meli, M., Olivieri, M., Romagnoli, C., 2021. Sea–level change along the Emilia–Romagna Coast from tide gauge and satellite altimetry. Remote. Sens. 13, 97. http://dx.doi.org/10.3390/rs13010097.

Meli, M., Romagnoli, C., 2022. Evidence and implications of hydrological and climatic change in the reno and lamone river basins and Related Coastal areas (Emilia-Romagna, northern Italy) over the last century. Water 14, 2650. http://dx.doi.org/10.3390/w14172650.

Meli, M., Vecchi, E., Romagnoli, C., 2026. Shoreline evolution in a low-lying coastal region under anthropogenic influence. Mar. Geol. 492, 107679. http://dx.doi.org/10.1016/j.margeo.2025.107679.

Mollema, P., Antonellini, M., Gabbianelli, G., Laghi, M., Marconi, V., Minchio, A., 2011. Climate and water budget change of a Mediterranean coastal watershed, Ravenna, Italy. Environ. Earth Sci. 65, 257–276. http://dx.doi.org/10.1007/s12665-011-1088-7.

Neter, J., Kutner, M.H., Nachtsheim, C.J., Wasserman, W., 1996. Applied Linear Statistical Models, fourth ed. McGraw-Hill Professional Publishing, New York, USA.

Obara, C., Fletcher, C.H., Habel, S., McDonald, K., Yamamoto, K., 2025. Drainage failure and associated urban impacts under combined sea-level rise and precipitation scenarios. Sci. Rep. 15, 23436. http://dx.doi.org/10.1038/s41598-025-07332-8.

O'Neill, B.C., Kriegler, E., Ebi, K.L., Kemp-Benedict, E., Riahi, K., Rothman, D.S., van Ruijven, B.J., van Vuuren, D.P., Birkmann, J., Kok, K., Levy, M., Solecki, W., 2017. The roads ahead: Narratives for shared socioeconomic pathways describing world futures in the 21st century. Glob. Environ. Chang. 42, 169–180. http://dx.doi.org/10.1016/j.gloenvcha.2015.01.004.

Papalexiou, S.M., Montanari, A., 2019. Global and regional increase of precipitation extremes under global warming. Water Resour. Res. 55 (6), 4901–4914. http://dx.doi.org/10.1029/2018WR024067.

Pavan, V., Antolini, G., Barbiero, R., Berni, N., Brunier, F., Cacciamani, C., Cagnati, A., Cazzuli, O., Cicogna, A., De Luigi, C., Di Carlo, E., Francioni, M., Maraldo, L., Marigo, G., Micheletti, S., Onorato, L., Panettieri, E., Pellegrini, U., Pelosini, R., Piccinini, D., Ratto, S., Ronchi, C., Rusca, L., Sofia, S., Stelluti, M., Tomozeiu, R., Torrigiani Malaspina, T., 2019. High resolution climate precipitation analysis for north-central Italy. Clim. Dyn. 52, 3435–3453. http://dx.doi.org/10.1007/s00382-018-4337-6.

Perini, L., Calabrese, L., Luciani, P., Olivieri, M., Galassi, G., Spada, G., 2017. Sea-level rise along the Emilia-Romagna coast (northern Italy) in 2100: Scenarios and impacts. Nat. Hazards Earth Syst. Sci. 17, 2271–2287. http://dx.doi.org/10.5194/nhess-17-2271-2017.

Preti, M., Nigris, N.D., Morelli, M., Monti, M., Bonsignore, F., Aguzzi, M., 2008. Stato del litorale emiliano–romagnolo all'anno 2007 e piano decennale di gestione. I quaderni di Arpa, p. 272, (In Italian).

Schwarz, G., 1978. Estimating the dimension of a model. Ann. Stat. 6 (2), 461–464, URL http://www.jstor.org/stable/2958889.

Shang, S., Wang, L., Li, X., Wu, L., Liu, Y., Su, X., Wang, L., Liu, G., 2025. Understanding cross-regional mutual influence mechanisms driven by polder drainage capacity changes in plain river network areas. Geomat. Nat. Hazards Risk 16 (1), 2582027. http://dx.doi.org/10.1080/19475705.2025.2582027.

Soboyejo, L.A., Giambastiani, B.M.S., Molducci, M., Antonellini, M., 2021. Different processes affecting long-term ravenna coastal drainage basins (Italy): implications for water management. Environ. Earth Sci. 80 (493), http://dx.doi.org/10.1007/s12665-021-09774-5.

Syvitski, J., Angel, J., Saito, Y., Overeem, I., Vörösmarty, C., Wang, H., Olago, D., 2022. Earth's sediment cycle during the anthropocene. Nat. Rev. Earth Environ. 3, 179–196. http://dx.doi.org/10.1038/s43017-021-00253-w.

Teatini, P., Ferronato, M., Gambolati, G., Bertoni, W., Gonella, M., 2005. A century of land subsidence in Ravenna, Italy. Environ. Geol. 47, 831–846. http://dx.doi.org/10.1007/s00254-004-1215-9.

Teatini, P., Ferronato, M., Gambolati, G., Gonella, M., 2006. Groundwater pumping and land subsidence in the Emilia–Romagna coastland, Italy: Modeling the past occurrence and the future trend. Water Resour. Res. 42 (1), http://dx.doi.org/10.1029/2005WR004242.

Teatini, P., Tosi, L., Strozzi, T., 2011. Quantitative evidence that compaction of holocene sediments drives the present land subsidence of the Po Delta, Italy. J. Geophys. Res.: Solid Earth 116 (B8), http://dx.doi.org/10.1029/2010JB008122.

Titus, J.G., Kuo, C.Y., Gibbs, M.J., LaRoche, T.B., Webb, M.K., Waddell, J.O., 1987. Greenhouse effect, sea level rise, and coastal drainage systems. J. Water Resour. Plan. Manag. 113 (2), 216–227. http://dx.doi.org/10.1061/(ASCE)0733-9496(1987)113:2(216).

Torres, M.E., Colominas, M.A., Schlotthauer, G., Flandrin, P., 2011. A complete ensemble empirical mode decomposition with adaptive noise. In: 2011 IEEE International Conference on Acoustics, Speech and Signal Processing. ICASSP, pp. 4144–4147. http://dx.doi.org/10.1109/ICASSP.2011.5947265.

Tosi, L., Teatini, P., Strozzi, T., Carbognin, L., Brancolini, G., Rizzetto, F., 2010. Ground surface dynamics in the northern adriatic coastland over the last two decades. Rend. Lincei. Sci. Fis. E Nat. 21, 115–129. http://dx.doi.org/10.1007/s12210-010-0084-2.

Turc, L., 1951. Nouvelles formules pour le bilan de l'eau en fonction des valeurs moyennes annuelles des précipitations et de la température. C. R. L'Acad. Sci. 233, 633–635, (In French).

Valente, M., Del Prete, C., Facci, G., Martino, A., Grilli, G.R., Bravi, F., Reno, C., Ragazzoni, L., 2025. The 2023 floods in the Emilia-Romagna Region, Italy: A retrospective qualitative investigation into response strategies and criticalities. Int. J. Disaster Risk Reduct. 116, 105089. http://dx.doi.org/10.1016/j.ijdrr.2024.105089.

Verberne, M., Teatini, P., Koster, K., Fokker, P., Zoccarato, C., 2025. An integral approach using InSAR and data assimilation to disentangle and quantify multi-depth driven subsidence causes in the Ravenna coastland, northern Italy. Geomech. Energy Environ. 43, 100710. http://dx.doi.org/10.1016/j.gete.2025.100710.

Vlotman, V.F., Smedema, L.K., Rycroft, D.W., 2020. Modern Land Drainage: Planning, Desing and Management of Agricultural Drainage Systems. CRC Press/Balkema, Taylor & Francis Group, Leiden, The Netherlands, http://dx.doi.org/10.1201/9781003025900-2.

Wahl, T., Jain, S., Bender, J., Meyers, S.D., Luther, M.E., 2015. Increasing risk of compound flooding from storm surge and rainfall for major US cities. Nat. Clim. Chang. 5, 1093–1097. http://dx.doi.org/10.1038/nclimate2736.

Wong, P.P., Losada, I.J., Gattuso, J.P., Hinkel, J., Khattabi, A., McInnes, K.L., Saito, Y., Sallenger, A., 2014. Coastal systems and low-lying areas. In: Field, C.B., Barros, V.R., Dokken, D.J., Mach, K.J., Mastrandrea, M.D., Bilir, T.E., Chatterjee, M., Ebi, K.L., Estrada, Y.O., Genova, R.C., Girma, B., Kissel, E.S., Levy, A.N., MacCracken, S., Mastrandrea, P.R., White, L.L. (Eds.), Climate Change 2014: Impacts,Adaptation, and Vulnerability. Part a: Global and Sectoral Aspects. Contribution of Working Group II to the Fifth Assessment Report of the Intergovernmental Panel on Climate Change. Cambridge University Press, pp. 361–409.

Yuan, C., Hu, Z., Liu, Y., He, S., Du, J., 2023. Application of ICEEMDAN to noise reduction of near-seafloor geomagnetic field survey data. J. Appl. Geophys. 209, 104933. http://dx.doi.org/10.1016/j.jappgeo.2023.104933.